ADVANCES IN ATMOSPHERIC SCIENCES, VOL. 30, NO. 1, 2013, 77–88

TRMM-retrieved Cloud Structure and Evolution of MCSs over the Northern South China Sea and Impacts of CAPE and Vertical Wind Shear

LI Xiangshu[1,2,4] (李香淑), GUO Xueliang*[2,3] (郭学良), and FU Danhong[2] (付丹红)

[1] *Cold and Arid Regions Environmental and Engineering Research Institute, Chinese Academy of Sciences, Lanzhou* 730000

[2] *Laboratory of Cloud and Precipitation and Severe Storms, Institute of Atmospheric Physics, Chinese Academy of Sciences, Beijing* 100029

[3] *Chinese Academy of Meteorological Sciences, Beijing* 100081

[4] *University of Chinese Academy of Sciences, Beijing* 100049

(Received 12 March 2012; revised 1 April 2012)

ABSTRACT

Cloud structure and evolution of Mesoscale Convective Systems (MCSs) retrieved from the Tropical Rainfall Measuring Mission Microwave Imager (TRMM TMI) and Precipitation Radar (PR) were investigated and compared with some pioneer studies based on soundings and models over the northern South China Sea (SCS). The impacts of Convective Available Potential Energy (CAPE) and environmental vertical wind shear on MCSs were also explored.

The main features of MCSs over the SCS were captured well by both TRMM PR and TMI. However, the PR-retrieved surface rainfall in May was less than that in June, and the reverse for TMI. TRMM-retrieved rainfall amounts were generally consistent with those estimated from sounding and models. However, rainfall amounts from sounding-based and PR-based estimates were relatively higher than those retrieved from TRMM-TMI data. The Weather Research and Forecasting (WRF) modeling simulation underestimated the maximum rain rate by 22% compared to that derived from TRMM-PR, and underestimated mean rainfall by 10.4% compared to the TRMM-TMI estimate, and by 12.5% compared to the sounding-based estimate. The warm microphysical processes modeled from both the WRF and the Goddard Cumulus Ensemble (GCE) models were quite close to those based on TMI, but the ice water contents in the models were relatively less compared to that derived from TMI.

The CAPE and wind shear induced by the monsoon circulation were found to play critical roles in maintaining and developing the intense convective clouds over SCS. The latent heating rate increased more than twofold during the monsoon period and provided favorable conditions for the upward transportation of energy from the ocean, giving rise to the possibility of inducing large-scale interactions.

Key words: TRMM, cloud structure and evolution, MCSs, South China Sea

Citation: Li, X. S., X. L. Guo, and D. H. Fu, 2013: TRMM-retrieved cloud structure and evolution of MCSs over the northern South China Sea and impacts of CAPE and vertical wind shear. *Adv. Atmos. Sci.*, **30**(1), 77–88, doi: 10.1007/s00376-012-2055-2.

1. Introduction

The East Asian monsoon is an important atmospheric system in summertime in eastern Asia. Its onset is known to initiate over the northern South China Sea (SCS), and is usually linked to flooding and drought in the region, and thus a lot of attention has been devoted to its formation and development

*Corresponding author: GUO Xueliang, guoxl@mail.iap.ac.cn

by atmospheric scientists. Some previous studies have shown that summer monsoon onset is closely associated with the rapid formation of mesoscale convective systems (MCSs) and their precipitation processes, as well as with diabatic heating processes over the SCS region (e.g. Hiragana et al., 1995; Lau and Yang, 1997; Wang, 2004; Johnson et al., 2005).

In order to investigate the physical mechanisms responsible for the onset and evolution of the East Asian summer monsoon, an international joint field experiment, SCSMEX, was conducted over the SCS and its surrounding areas in 1998, in particular during two intensive observation periods (IOPs) on 5–25 May and 5–25 June 1998 (Lau et al., 2000). Ding and Liu (2001) pointed out that the onset and development of the summer monsoon over the SCS in 1998 could be divided into three periods: beginning 15 May, low-level southwesterly winds from the tropics prevailed in the northern SCS; then, by 20 May, low-level southwesterly monsoon flow dominated over the whole of the SCS; and finally, upper-level northeasterly winds prevailed by 23–24 May.

The relationship between monsoon wind flow and the formation and evolution of MCSs over the SCS has been investigated using intensive sounding, radar and satellite data, as well as numerical cloud models (Johnson and Ciesielski, 2002; Tao et al., 2003; Wang, 2004; Wang and Carey, 2005; Wang et al., 2007). It was found that monsoon onset started in mid-May and was accompanied by a rapid increase in deep convections over a period of one week to ten days, followed by a 10-day break, and then deep convections again for a week-to-ten-day period in early June. Due to greater heating and moistening rates, as well as higher vertical eddy flux during the early-June of the monsoon active period than those observed during the May of the monsoon onset period, the indication was that more vigorous deep convections were induced by monsoon activity.

Lin and Kueh (2003) utilized the Mesoscale Model 5 (MM5) to diagnose the occurrence and evolution of MCSs during 15–25 May, and suggested that latent heating would further induce the development of new mesoscale convection. Tao et al. (2003) used the 2-D Goddard Cumulus Ensemble (GCE) model to simulate convections and found that the temporal variation in the modeled rainfall, mean heating and moisture budgets were consistent with soundings-based estimates. However, the model underestimated rainfall by 17%–20% compared to sounding-based estimates, although it agreed better with observations for June than those for May. Wang (2004) investigated the convective systems related to subtropical frontal passages in the early onset of the Southeast Asian monsoon using dual-Doppler radar data, and suggested that the interaction between the tropical monsoon flow and frontal circulation was important for the evolution and structure of MCSs. Meanwhile, due to the moderate vertical wind shear, a straight updraft pattern was found in the prefrontal convections.

Liu and Ding (2005) and Liu et al. (2005) found that favorable synoptic and dynamic conditions were produced by the large-scale background for the formation and evolution of MCSs. In addition, the formation of mesoscale convective activities also produced an obvious feedback effect on large-scale circulations by the release of latent heating. Wang et al. (2007) investigated the evolution, dynamic structure and cloud microphysics, as well as rainfall processes, of monsoon convections over the SCS using a 2-D cloud-resolving simulation combined with dual-Doppler and polarimetric radar data, and found that the model results showed many similarities to observed data. Fu et al. (2011) investigated the effects of cloud microphysics on SCS monsoon convective systems based on a 2-D cloud-resolving model, and found that ice microphysics can produce less rain prior to and during the onset of the monsoon period, and the effect of ice microphysics on precipitation is dominated by radiation processes instead of microphysics itself.

Since most recent studies have focused on large-scale wind flow and radar echo structure and evolution of MCSs over the SCS based on data obtained during IOPs, cloud microphysical data are scarce due to a lack of relevant measurements. In addition, the limited ground-based radar data available cannot provide detailed analyses of the cloud structure of MCSs. Thus, a detailed picture of cloud microphysical structure and evolution of MCSs responding to the onset and development of the Southeast Asian monsoon over the SCS, which is critical for revealing cloud and precipitation formation mechanisms, cannot be precisely obtained.

In this paper, Tropical Rainfall Measuring Mission (TRMM) data, including Precipitation Radar (PR) and TRMM Microwave Imager (TMI) and sounding data, four times a day in May and June, are used to investigate the structure and evolution of MCS cloud microphysics. The TRMM-derived results are compared against some pioneer sounding-based works (e.g. Johnson and Ciesielski, 2002) and modeled results (e.g. Tao et al., 2003; Wang et al., 2007; Fu et al., 2011). The impacts of environmental wind shear and thermodynamics on the formation and evolution of MCSs before and after the onset of the summer monsoon over the SCS are also addressed. The paper is organized as follows: following this introduction, section 2 describes the data used in the study. Section 3 reports the cloud

microphysical structure and evolution of monsoon convections derived from TRMM data. The effects of Convective Available Potential Energy (CAPE) and wind shear on MCSs are described in section 4, before conclusions being drawn in the final section, section 5.

2. Data

Tropical Rainfall Measuring Mission Microwave Imager (TRMM TMI) and Precipitation Radar (PR) standard scanning orbit data recorded during SCSMEX were used in this study. This included the TRMM Precipitation Radar (PR) Level 2 Rainfall Rate and Profile Product (TRMM Product 2A25) dataset, which was corrected for the rain attenuation in measured radar reflectivity, and used to estimate the instantaneous 3-D distribution of rain from the PR data. The TRMM Microwave Imager (TMI) Level 2 Hydrometeor Profile Product (TRMM Product 2A12) TMI dataset was also used. The data were able to provide vertical profiles of hydrometeor surface rain at 14 vertical levels based on TMI brightness temperatures. The 3-Hourly TRMM Precipitation Estimates (3B42) dataset was generated from calibrated TRMM-adjusted merged-infrared IR data merged with TRMM and other satellite data. The resolution of the dataset was $0.25^\circ \times 0.25^\circ$ grid boxes every 3 h.

The data used in this study were derived partly from the South China Sea Monsoon Experiment (SCSMEX) (Ding et al., 1999; Lau et al., 2000). Two IOPs were conducted during the field observation of 5–25 May and 5–25 June 1998. The observed data included meteorological observations, oceanographic observations, radar and satellite data, and precipitation data. The study area is shown in Fig. 1.

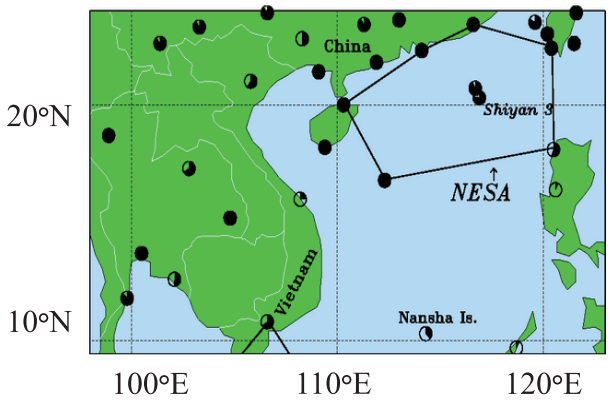

Fig. 1. Northern Enhanced Sounding Array (NESA) of SCS during the IOPs of SCSME.

3. Cloud microphysical structure and the evolution of monsoon convections over the SCS

3.1 *Satellite images and TRMM-PR radar reflectivity*

The cold frontal passages from northwestern China to the coastal regions were observed periodically at intervals of 2–4 days from the beginning of the observation period on 5 May 1998. An example of this type of frontal cloud band on 11 May showed that before monsoon onset the cloud bands associated with the frontal system weakened and dissipated while it passed over the coast of China and on into the northern SCS (Figs. 2a and b). After the onset of monsoon on 15 May, the frontal cloud band that moved over the sea from the coastal region was not weakened, but enhanced and developed into a pronounced frontal cloud band oriented from southwest to northeast, which covered most coastal regions of southeastern China (Figs. 2c and d).

Figure 3 shows the time evolutions of vertical maximum reflectivity of the cloud systems and maximum rain rate based on TRMM-PR data before and after the onset of summer monsoon over the northern SCS. It shows that before the onset of summer monsoon, the maximum radar echo intensity and the echo top were low (Fig. 3a), indicating that the deep convective system had not yet developed. After monsoon onset, the radar echo increased rapidly, and the echo tops reached close to 20 km. During 25–31 May, the convective systems decreased, while after 1 June, the convection again developed and intensified over a period of one week to ten days. The reflectivity derived from PR on TRMM showed a relatively stable development and evolution of convections after the onset of monsoon, except for the period from 31 May to 2 June, during which the convections weakened. The maximum radar reflectivity was around 50 dBZ, which was primarily located at levels below 6 km and occurred during the two active periods of convections, and slightly less than the 55 dBZ obtained by ground-based C-band polarimetric/Doppler (C-POL) radar (Wang et al., 2007). The characteristics of convections derived from TRMM-PR data during SCSMEX were in good agreement with previous studies (Johnson and Ciesielski, 2002; Tao et al., 2003; Johnson et al., 2005; Wang et al., 2007; Fu et al., 2011). In their works, two convectively active periods were also identified by observations and simulations. Also, a relatively stable development of convections was found after the onset of monsoon, except for the period between 31 May and 2 June.

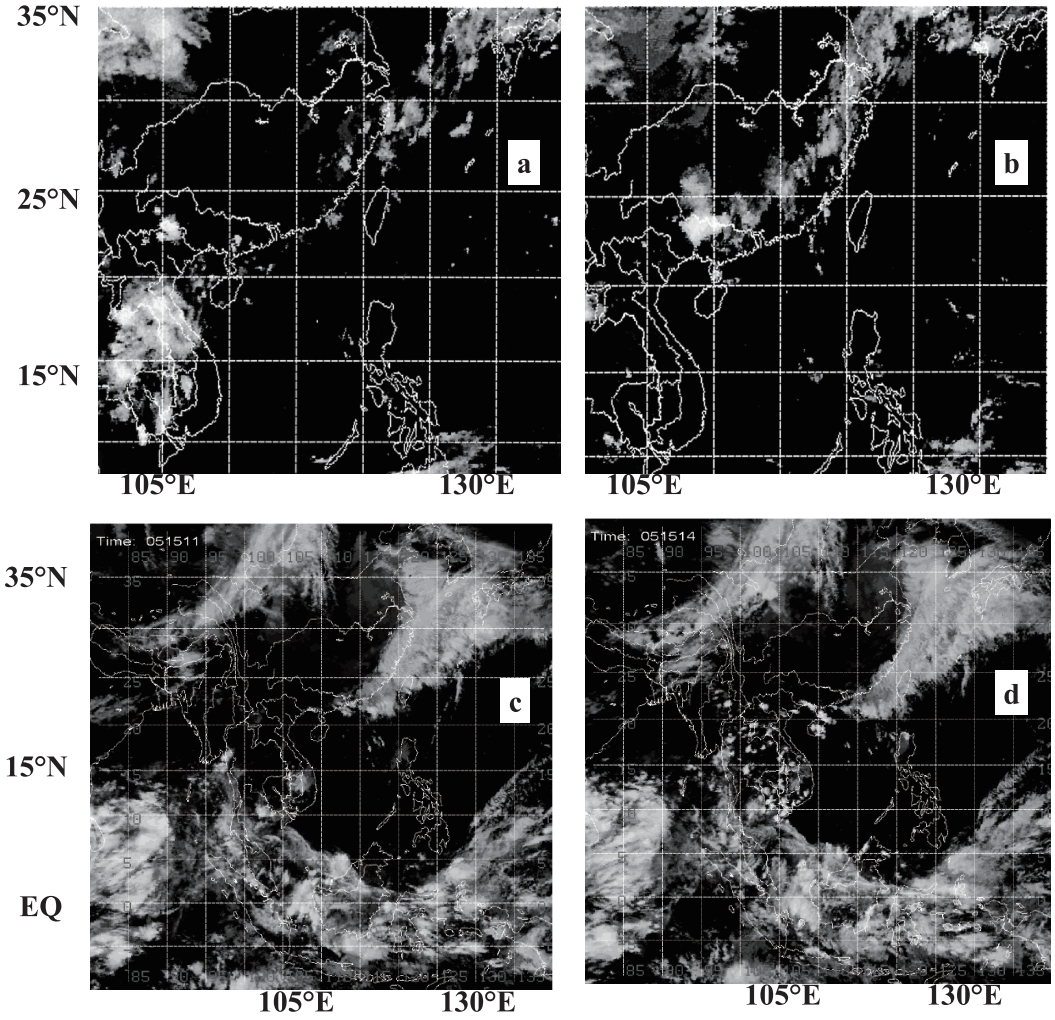

Fig. 2. Infrared imagery from Geostationary Meteorological Satellite-5 (GMS-5) over the South China Sea (30°N–10°S, 95°–180°E) (a) 0800 LST 11 May, (b) 2300 LST 11 May, (c) 1100 LST 15 May, (d) 1400 LST 15 May.

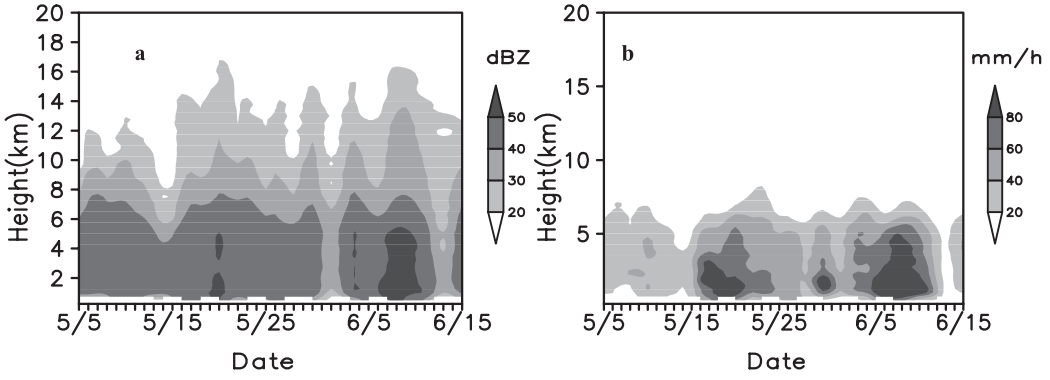

Fig. 3. Time–height distributions of (a) the maximum reflectivity and (b) the maximum rain rate based on Precipitation Radar (PR) before and after the onset of summer monsoon over the northern SCS (15°–25°N, 108°–122°E).

The height–time distribution of maximum rain rate (Fig. 3b) suggests that little precipitation was produced over the SCS before 15 May, while during 15–25 May the convections were very active and the maximum rain rate reached 90–110 mm h^{-1}. Then, precipitation gradually decreased, and after 2 June the convection and precipitation intensified again, and the maximum rain rate exceeded 110 mm h^{-1}. The Weather Research and Forecasting (WRF)-based simulation underestimated the maximum rain rate by 22% compared to that derived from TRMM-PR. The simulated maximum rain rate basically ranged between 70–80 mm h^{-1} (Fu et al., 2011).

3.2 *TRMM-TMI cloud microphysical characteristics*

To understand the microphysical structure of the convective clouds before and after the onset of the summer monsoon, Fig. 4 displays the microphysical structures of the convective clouds retrieved from TRMM-TMI data over the SCS before and after the onset of the summer monsoon. Both non-precipitating and precipitating cloud water and cloud ice were relatively less abundant before the onset of monsoon, while after the onset they obviously increased in intensity and area. Small-scale intensive convections were very active within the mesoscale convections, and convective clouds featured long-lasting development. The melting level was located close to 5.5 km. Figure 4 also shows that the distributions of higher cloud water (Fig. 4a) and rain water (Fig. 4c) corresponded very well to that of higher precipitating ice content at the upper level (Fig. 4d), which indicates that ice processes were active in precipitation production. Maximum cloud water and cloud ice reached more than 0.6 g m^{-3} and 0.16 g m^{-3}, respectively, the latter being mainly located at 15–16 km. Maximum precipitating ice content sometimes reached more than 1.4 g m^{-3}, was mainly distributed near the melting level, and was strongly associated with water-phase precipitation.

Comparing the cloud microphysical properties retrieved from TRMM-TMI to those from models, the warm microphysical processes modeled by WRF, such as distribution and amounts, were quite close to those based on TMI data, but the ice water content in the models were relatively less than those derived from TMI data (Fu et al., 2011). This might be an important reason why modeled rainfall maxima were less than that from TRMM estimates, although mean rain-

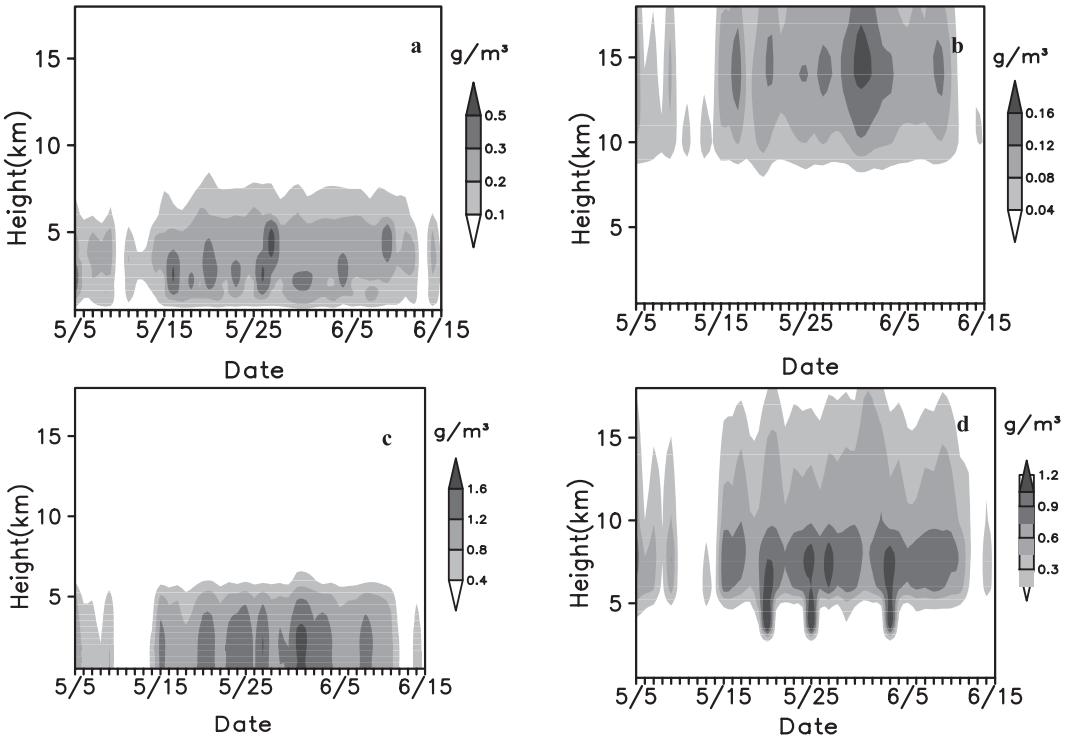

Fig. 4. Time–height distributions of the maximum (a) cloud water content, (b) cloud ice content, (c) rain water, and (d) precipitation ice-phase particles based on TMI before and after the onset of summer monsoon over the northern SCS (15°–25°N, 108°–122°E).

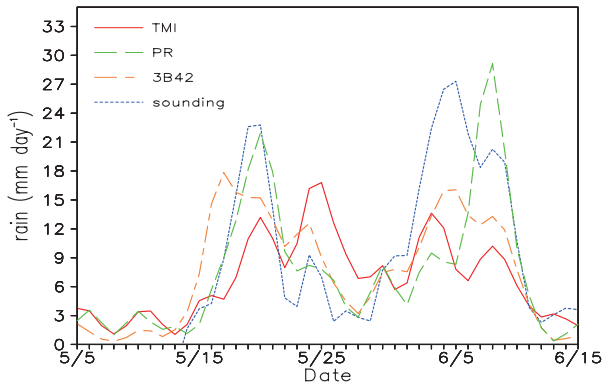

Fig. 5. Time series of domain-averaged surface rainfall amounts (mm d^{-1}) retrieved from TMI and PR, and estimated from sounding. The mean rainfall from TRMM 3B42 data is also shown.

fall values were more consistent.

3.3 *TRMM TMI- and PR-retrieved surface rainfall*

Figure 5 displays time series of domain-averaged surface rainfall obtained from TRMM PR and TMI-based estimates, sounding-based estimates, as well as estimates based on the TRMM 3B42 dataset in the Northern enhanced sounding array (NESA) area. It shows that the domain-averaged surface rainfall estimated from different sources was generally consistent in reflecting two typical convections responding to the onset of monsoon. However, large differences are evident if the rainfall amounts and peaks derived from different methods are compared. The rainfall peaks estimated from both TRMM-PR and sounding are higher than those from TRMM-TMI results. The PR-retrieved rainfall in May was less than that in June, and the reverse for TMI. The reason is unclear, but recent studies (e.g. Robertson et al., 2003) showed that the assumed drop size distribution and associated attenuation/reflectivity/rainfall relationships inherent in single-frequency radar methods are serious issues, even for the improved algorithm (Shige et al., 2006). TMI-estimated rainfall seemed to be better compared to that from PR (e.g. Robertson et al., 2003). When comparing the surface mean rainfall estimated from TMI with that derived from the TRMM-3B42 dataset in Fig. 5, we can see that the TMI-retrieved rainfall amount was more consistent with that obtained from the TRMM 3B42 dataset, which was a three-hourly dataset derived from combinations of PR, TMI and other sources.

The soundings-estimated surface rainfall rates were generally in good agreement with those retrieved from TRMM, in particular after some corrections (Johnson and Ciesielski, 2002; Fu et al., 2011). However, a study by Tao et al. (2003) showed that the sounding-estimated mean surface rainfall rate was higher than that from PR and less than that from TMI. Our study also shows that the sounding-estimated mean rainfall was quite close to that of TMI- and PR-estimated rainfall in May, but not in June.

The modeled properties of rainfall in the study region, such as peaks and time series, were generally in good agreement with those retrieved from TRMM (Tao et al., 2003; Wang et al., 2007; Fu et al., 2011). However, there were also many differences between modeled and TRMM-retrieved rainfall amounts. It should be noted that different modeling studies used different domains, and even if the differences in domain area were small, the averaged rainfall might be large, especially for convective clouds. Therefore, precise comparisons between different modeled rainfall results and TRMM data are difficult. To be more objective, data from both published papers and from this study were used and compared. Tao et al. (2003) noted that GCE model-simulated rainfall returned better results for June than May, underestimated rainfall by 17%–20% compared to sounding estimates, and showed very good agreement with PR estimates, but less so with TMI estimates. Surprisingly, in this study, the GCE-modeled rainfall rate was quite accurate for May, but less so for June compared to TMI estimates. This is because the TMI-estimated rainfall reported by Tao et al. (2003) was larger than that found in the present study; plus, our study showed similar results for the rainfall rate between GCE-modeled and PR-estimated results. All data are listed in Table 1.

Based on the modeling study by Fu et al. (2011), the WRF underestimated mean rainfall by 10.4% compared to the TRMM-TMI estimate, and by 12.5% compared to the sounding estimate. The simulated mean rainfall was reasonably consistent with that from

Table 1. Domain-averaged surface rainfall amounts (mm d^{-1}) for both the May and June cases, retrieved by TRMM PR and TMI, and estimated from soundings and the GCE model.

	TMI-based rainfall	PR-based rainfall	Sounding-based rainfall	3B42-based rainfall	GCE-modeled rainfall
18–26 May1998	11.71	12.49	11.20	11.95	11.14
2–11 Jun 1998	9.36	14.05	19.09	12.07	16.46

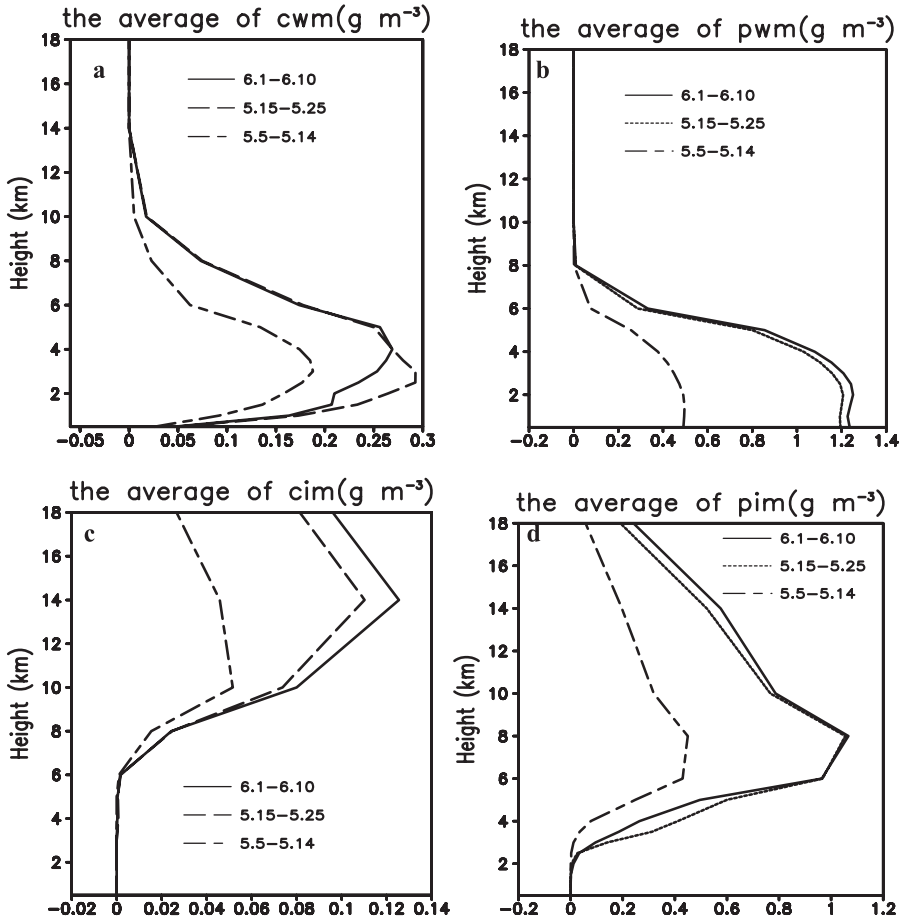

Fig. 6. Profiles of cloud hydrometeors during pre-onset (5–14 May, dashed lines), onset (15–25 May, dotted lines) and post-onset (1–10 June, solid lines), (a) cloud water, (b) rain water, (c) cloud ice, and (d) precipitation ice-phase particles based on TRMM TMI over the northern SCS.

TMI in the case of May, but higher for June. Plus, the evolution tendency of simulated rainfall was quite close to the sounding-based estimate in both periods. The ice microphysical process derived from the WRF model was more consistent with that derived from TMI. John et al. (2009) pointed out that the discrepancies between variability in precipitation were not only between models and observations, but also between the observational estimates themselves, and thus improvements in the observation system were required.

The profiles of cloud hydrometeors during pre-onset (5–14 May), onset (15–25 May) and post-onset (1–10 June) based on TRMM-TMI over the northern SCS are displayed in Fig. 6. It shows that large differences between pre-onset and onset (post-onset) could be found in amount and vertical distributions of cloud hydrometeors. Owing to the rapidly intensified convections during onset and post-onset of the monsoon, ice-phase processes became active and important to precipitation production.

3.4 *Microphysical structure of individual clouds*

To better understand the microphysical structure and evolution of individual clouds, the TMI data of the surface rain rate on 15 May over the northern SCS are shown in Fig. 7. It clearly shows that the convective clouds that moved from southern China to the northern SCS from 1040 LST to 1710 LST on 15 May were intensified and produced the heavy rain (Figs. 7a and b).

The vertical cross sections of hydrometeors along lines AB and CD in Fig. 7 are shown in Figs. 8 and 9, respectively. The mesoscale convective clouds had obviously been intensified after moved to the northern SCS, which had characteristics of multi-cellular structure, and the hydrometeor content increased. The max-

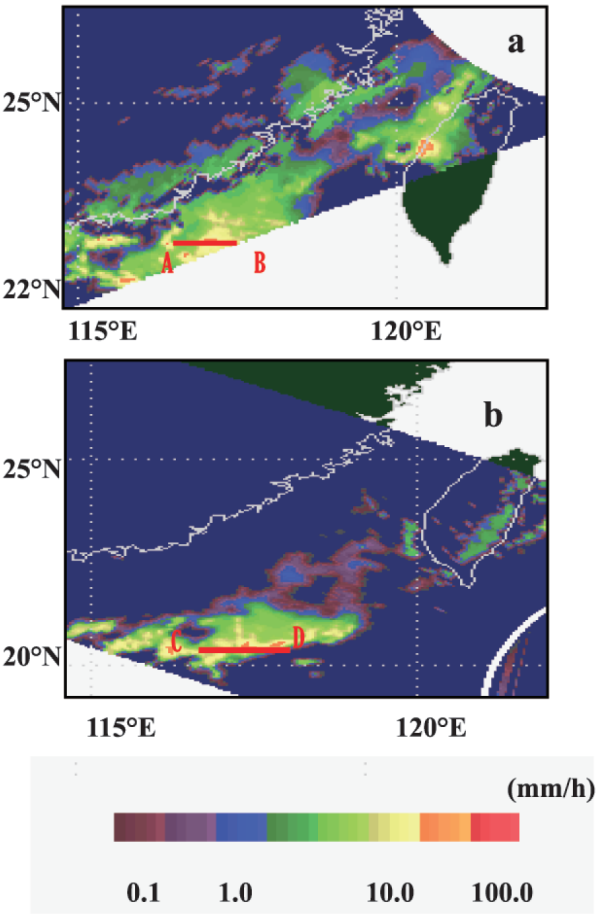

Fig. 7. The surface rain rate observed by TMI on 15 May over the northern SCS (a) 2653 orbit (1041 LST–1044 LST), (b) 2657 orbit (1710 LST–1713 LST).

imum cloud water content was about 0.15–0.2 g m^{-3}, and a great amount of the supercooled cloud water existed above the melting level near 5.5 km, which was favorable for the formation of the precipitation particles (Figs. 8a and 9a). Maximum rainwater reached 1.6 g m^{-3} and was mainly located below the melting levels (Figs. 8b and 9b). Budget calculation for cloud particles showed that the transformation of cloud water to rainwater only accounted for 30% of precipitation water. Melting of ice particles accounted for 70% of precipitation water, indicating that the rainwater mainly came from the melting of the ice particles.

The maximum cloud ice content was about 0.1 g m^{-3} near 14 km, and the cloud ice still existed above 18 km, which showed that the convective clouds were deep and intense (Figs. 8c and 9c). The maximum precipitation ice-phase particles reached 1.0 g m^{-3} near the melting levels, which was the main source of rainwater (Figs. 8d and 9d).

During the period of eastward movement of the MCSs, the multi-cellular cloud bands were weakened and reduced in Fig. 9 relative to those in Fig. 8.

4. The effects of CAPE and wind shear on MCSs

CAPE and vertical wind shear have been found to play important roles in the formation and development of oceanic convection, and were calculated in this study to check their effects on MCSs before and after monsoon onset over the SCS region. Equations (4) and (5), respectively, were used for this purpose.

$$\mathrm{CAPE} = g \int_{\mathrm{LFC}}^{\mathrm{EL}} \frac{T_{\mathrm{v,p}} - T_{\mathrm{v,e}}}{T_{\mathrm{v,e}}} \mathrm{d}z \,, \tag{1}$$

where EL is the equilibrium level; LFC is the level of free convection height; $T_{\mathrm{v,p}}$ is the virtual temperature of the specific parcel; $T_{\mathrm{v,e}}$ is the virtual temperature of the environment; and g is the acceleration due to gravity.

Vertical wind shear is commonly classified as "directional" or "speed" shear (Weisman and Klemp, 1982, 1986; Markowski and Richardson, 2006). Observational studies (e.g. Rasmussen and Blanchard, 1998) have confirmed that vertical wind shear over the lowest 6 km AGL is important for the formation of strong convections. Here, the bulk shear, which refers to the magnitude of the bulk vector difference (top minus bottom) divided by depth (Thompson et al., 2007), was used. The bulk vector difference between the mean wind in the lowest 500 m and the lowest 6 km was simply defined as:

$$S = \left(\sqrt{(\overline{u}_{6.0}^2 + \overline{v}_{6.0}^2)} - \sqrt{(\overline{u}_{0.5}^2 + \overline{v}_{0.5}^2)} \right) / (H_{6.0} - H_{0.5}) \,, \tag{2}$$

where S is the wind shear (units: s^{-1}); $\overline{u}_{6.0}$ and $\overline{v}_{6.0}$ are the average horizontal wind speeds at 6 km height; and $\overline{u}_{0.5}$ and $\overline{v}_{0.5}$ are those at 0.5 km height. $H_{6.0}$ is 6 km and $H_{0.5}$ is 0.5 km.

Figures 10 and 11 show the temporal distribution of averaged CAPE and vertical wind shear over the northern SCS, respectively. CAPE and vertical wind shear showed obvious changes before and after the onset of the monsoon. Before the onset of the monsoon on 15 May, although the maximum CAPE reached 1900 J kg^{-1}, the vertical wind shear was very low. This is the reason why the convective clouds weakened and dissipated when passing over the SCS before the onset. After the onset of monsoon on 15 May, the CAPE remained at 1200 J kg^{-1} to 1400 J kg^{-1}, except during monsoon weakened days, and the maximum

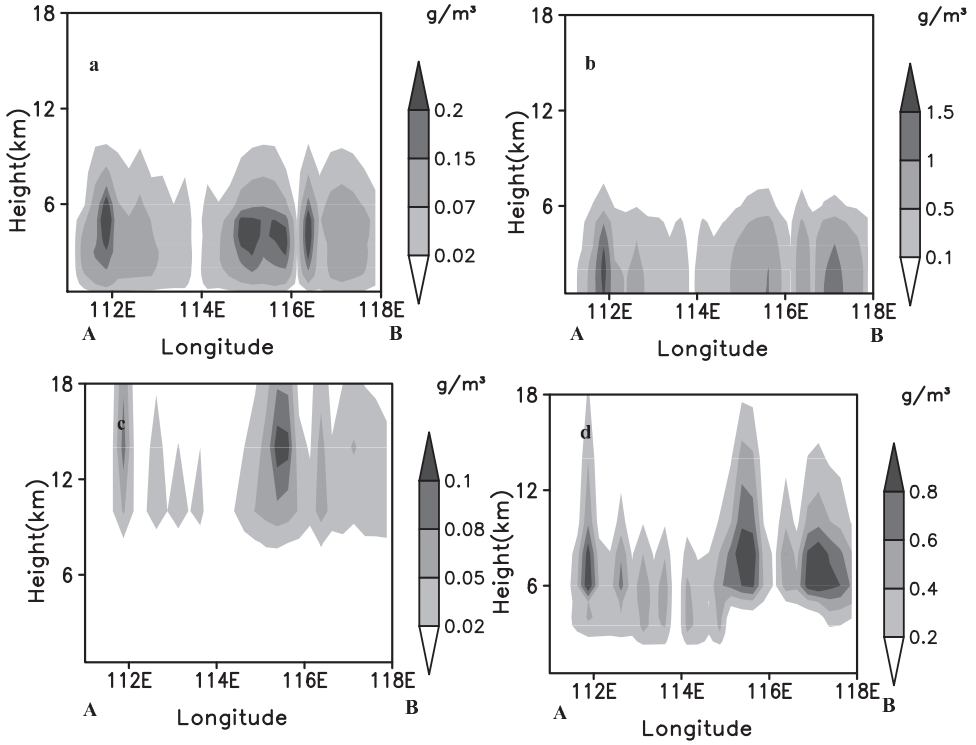

Fig. 8. Vertical cross sections of cloud hydrometeors along line AB (lat=22.37°N) (a) cloud water, (b) precipitation water, (c) cloud ice, and (d) precipitation ice (g m^{-3}).

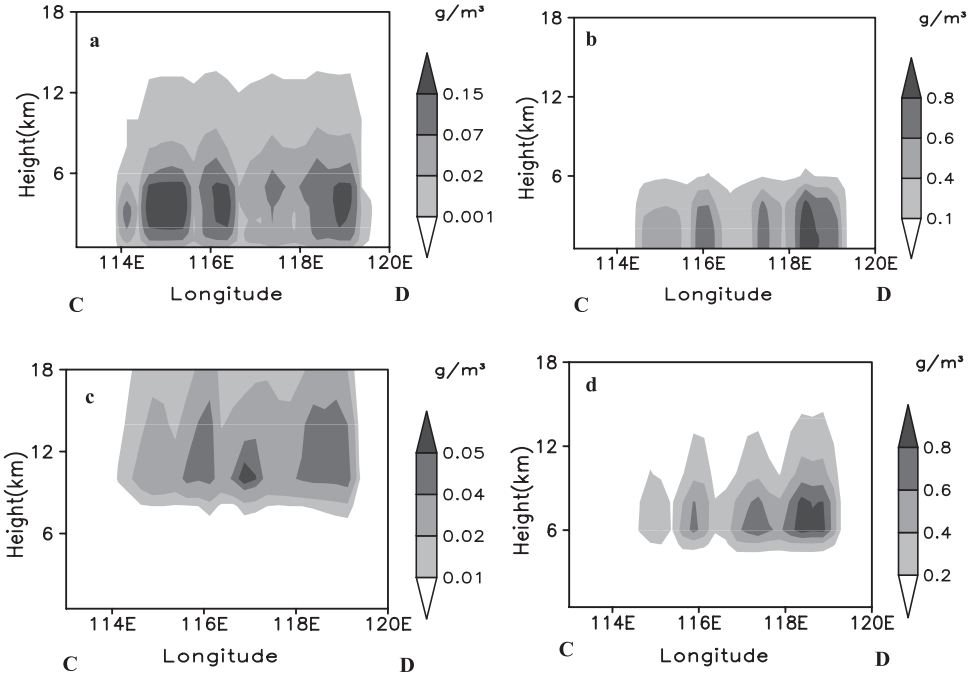

Fig. 9. As Fig. 8, but for the vertical cross sections along line CD (lat=20.875°N).

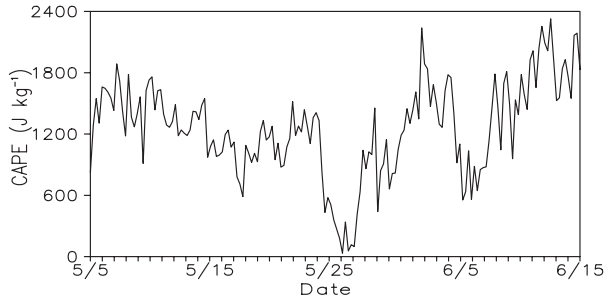

Fig. 10. Time evolution of the averaged CAPE (J kg^{-1}) over the northern SCS (15°–25°N, 108°–122°E) before and after the monsoon onset.

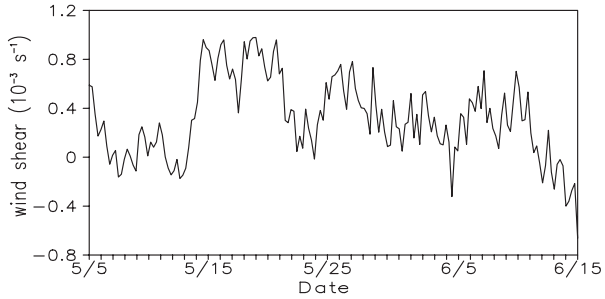

Fig. 11. Time evolution of the domain averaged vertical wind shear (10^{-3} s^{-1}) over the northern.

value reached 2300 J kg^{-1}, while the vertical wind shear increased.

To further discern how the vertical wind shear and CAPE were related with the formation and evolution of MCSs before and after the onset of monsoon over the SCS, Fig. 12 displays the relations of vertical wind shear and CAPE with the mean precipitation of MCSs. It shows that two prominent precipitation periods between 15 and 25 May, and between 30 May and 10 June corresponded very well to the higher values of vertical shear and CAPE. Before monsoon onset, wind shear was too low, though CAPE was high, and little precipitation was produced. During the period 24–30 May, the CAPE decreased to its lowest value, though wind shear was still high, and precipitation dramatically decreased.

The time series of maximum vertical latent heat distribution in Fig. 13 shows that the release of latent heat due to the strong convection induced by the onset of monsoon was much larger than that before the onset. Before the onset, the phase transition of water vapor was weak due to the weak convective processes and the latent heating rate was also low. After the onset of monsoon, the latent heating rate increased more than twofold and reached the tropopause, meaning the

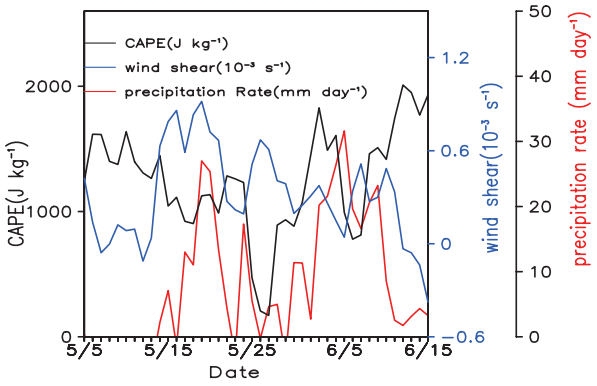

Fig. 12. Time evolutions of the domain averaged CAPE (J kg^{-1}), vertical wind shear (10^{-3} s^{-1}) and TRMM-estimated surface rain rate (mm d^{-1}) over the northern SCS.

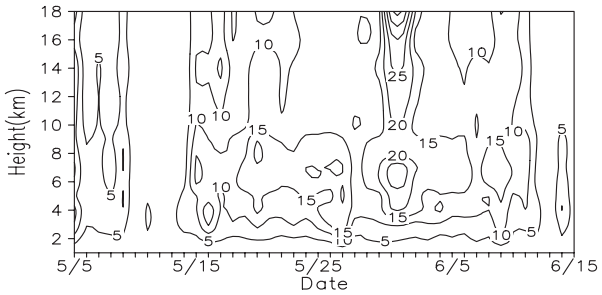

Fig. 13. Time evolution of the maximum latent heat (°C h^{-1}) over the northern SCS.

transportation of energy from ocean to upper atmosphere was possible during the monsoon active period. This process needs further investigation in a future study.

5. Summary and conclusions

The SCS summer monsoon onset was found to be closely associated with the rapid formation of MCSs and its precipitation processes. To understand the cloud microphysical structure and evolution of MCSs, including how it is related to the onset and development of the Southeast Asian Monsoon, is critical to reveal the precipitation processes and formation mechanisms of MCSs over the SCS.

By using TRMM PR and TMI data, as well as intensive sounding data from SCSMEX, the structure and evolution of MCSs were studied and compared against some pioneer sounding-based and modeled results. The effects of environmental CAPE and vertical wind shear on the formation and development of MCSs over the northern SCS were also investigated.

The cold frontal cloud system from the coastal region of South China started to weaken and dissipate while it entered the SCS before the onset of the East Asian Monsoon; then, after the onset, it intensified and developed as deeper and long-lasting MCSs with heavy precipitation formed. The maximum rain rate was able to reach 90–110 mm h^{-1} after the onset of monsoon. The WRF simulation underestimated the maximum rain rate by 22% compared to that derived from TRMM-PR data.

The cloud microphysical structures retrieved from TRMM-TMI showed that the distributions of higher cloud water and rainwater corresponded very well to that of higher precipitating ice content at the upper level, indicating that ice processes were active in precipitation production. Maximum cloud water and cloud ice reached more than 0.6 g m^{-3} and 0.16 g m^{-3}, respectively, the latter being mainly located at 15–16 km. The maximum precipitating ice content was sometimes more than 1.4 g m^{-3}, was mainly distributed near the melting level, and was strongly associated with water-phase precipitation. The transformation of cloud water to rainwater only accounted for 30% of precipitation water, while that from the melting of ice particles accounted for 70%.

The domain-averaged surface rainfall amounts from TMI and PR data were generally consistent. However, there were also some differences between TMI- and PR-retrieved rainfall. The PR-retrieved surface rainfall in May was less than that in June, and the reverse for TMI. The sounding-based surface rainfall rates were also generally in good agreement with those retrieved from TRMM data. However, on average, the rainfall amounts from sounding-based estimates were relatively higher than those retrieved from TRMM.

The GCE-modeled rainfall rate was reasonably accurate for May, but not for June – the reverse of that reported by Tao et al. (2003). Similar results for rainfall rates based on GCE modeling and PR estimates were obtained. The WRF underestimated mean rainfall by 10.4% compared to the TRMM-TMI estimate, and by 12.5% compared to the sounding-based estimate. WRF-modeled mean rainfall was pretty consistent with that from TMI in the case of May, but higher for June.

CAPE and vertical wind shear induced by the monsoon circulation played critical roles in maintaining and developing intense convective clouds over the SCS. The latent heating rate increased more than twofold during the monsoon period and provided favorable conditions for the upward transportation of energy from the ocean surface, thus generating possible impacts on the larger-scale system.

Acknowledgements. The authors are grateful for the critical and valuable comments from two anonymous reviewers, which greatly improved the quality of this paper. This study was jointly sponsored by the Chinese Natural Science Foundation (Grant Nos. 40575003 and 40333033) and the special foundation of the Chinese Academy of Meteorological Sciences (2011Z005).

REFERENCES

Ding, Y.-H., and Y. Liu, 2001: Onset and evolution of the summer monsoon over the south China sea during SCSMEX field experiment in 1998. *J. Meteor. Soc. Japan*, **79**(1B), 255–276.

Ding, Y. H., J. S. Xue, and S. R. Wang, 1999: Onset and activities of Asian monsoon and heavy flooding in China in 1998. *Onset and Evolution of the South China Sea Monsoon and Its Interaction with the Ocean.* Y. H. Ding and C. Y. Li, Eds., China Meteorological Press, Beijing, 193–199.

Fu, D., X. Guo, and C. Liu, 2011: Effects of cloud microphysics on monsoon convective system and its formation environments over the South China Sea: A two-dimensional cloud-resolving modeling study. *J. Geophys. Res.*, **116**, D07108, doi: 10.1029/2010JD014662.

Hiragana, H., K. Kato, and T. Takeda, 1995: Abrupt change in the characteristics of the cloud zone in subtropical East Asia around the middle of May. *J. Meteor. Soc. Japan*, **73**, 221–239.

John, V. O., R. P. Allan, and B. J. Soden, 2009: How robust are observed and simulated precipitation responses to tropical ocean warming? *Geophys. Res. Lett.*, **36**, L14702, doi: 10.1029/2009GL038276.

Johnson, R. H., and P. E. Ciesielski, 2002: Characteristics of the 1998 summer monsoon onset over the Northern South China Sea. *J. Meteor. Soc. Japan*, **80**, 561–578.

Johnson, R. H., L. A. Steven, and P. E. Ciesielski, 2005: Organization of oceanic convection during the onset of the 1998 East Asian summer monsoon. *Mon. Wea. Rev.*, **133**(1), 131–148.

Lau, K.-M., and S. Yang, 1997: Climatology and interannual variability of the southeast Asian summer monsoon. *Adv. Atmos. Sci.*, **14**(2), 141–162.

Lau, K. M., and Coauthors, 2000: Report of the field operations and early results of the South China Sea Monsoon Experiment (SCSMEX). *Bull. Amer. Meteor. Soc.,* **81**(6), 1261–1270.

Lin, S. C., and M. T. Kueh, 2003: A modeling diagnosis of the development of mesoscale convective system over South China Sea during the summer monsoon onset in 1998. *Terrestrial, Atmospheric and Oceanic Sciences*, **14**, 369–399.

Liu, Y.-J., Y.-H. Ding, and N. Zhao, 2005: A study on the mesoscale convective systems during the summer monsoon onset over the South China Sea in 1998. Part I: Analysis of large-scale fields for occurrence

and development of the mesoscale convective systems. *Acta Meteorologica Sinica*, **19**(3), 275–288.

Liu, Y.-J., and Y.-H. Ding, 2005: A study on the mesoscale convective systems during the summer monsoon onset over the South China Sea in 1998 Part II: Effect of mesoscale convective systems on large-scale fields. *Acta Meteorologica Sinica*, **19**(3), 289–301.

Markowski, P., and Y. Richardson, 2006: On the classification of vertical wind shear as directional shear versus speed shear. *Wea. Forecasting*, **21**, 242–247.

Rasmussen, E. N., and D. O. Blanchard, 1998: A baseline climatology of sounding-derived supercell and tornado forecast parameters. *Wea. Forecasting*, **13**, 1148–1164.

Robertson, F. R., D. E. Fitzjarrald, and C. D. Kummerow, 2003: Effects of uncertainty in TRMM precipitation radar path integrated attenuation on interannual variations of tropical oceanic rainfall. *Geophys. Res. Lett.*, **30**(4), 1180, doi: 10.1029/2002GL016416.

Shige, S., H. Sasaki, K. Okamoto, and T. Iguchi, 2006: Validation of rainfall estimates from the TRMM precipitation radar and microwave imager using a radiative transfer model: 1. Comparison of the version-5 and -6 products. *Geophys. Res. Lett.*, **33**, L13803, doi: 10.1029/2006GL026350.

Tao, W. -K., C.-L. Shie, J. Simpson, S. Braun, R. H. Johnson, and P. E. Ciesielski, 2003: Convective systems over the South China Sea: Cloud-resolving model simulations. *J. Atmos. Sci.*, **60**, 2929–2956.

Thompson, R. L., C. M. Mead, and R. Edwards, 2007: Effective storm-relative helicity and bulk shear in supercell thunderstorm environments. *Wea. Forecasting*, **22**, 102–114.

Wang, J. J., 2004: Evolution and structure of the mesoscale convection and its environment: A case study during the early onset of the Southeast Asian summer monsoon. *Mon. Wea. Rev.*, **132**(5), 1104–1132.

Wang, J.-J., and L. Carey, 2005: Structure and evolution of an oceanic squall line during the South China Sea Monsoon Experiment. *Mon. Wea. Rev.*, **133**, 1544–1561.

Wang, J.-J., X. F. Li, and L. Carey, 2007: Evolution, structure, cloud microphysical, and surface rainfall processes of monsoon convection during the South China Sea Monsoon Experiment. *J. Atoms. Sci.*, **64**, 360–380.

Weisman, M. L., and J. B. Klemp, 1982: The dependence of numerically simulated convective storms on vertical wind shear and buoyancy. *Mon. Wea. Rev.*, **110**, 504–520.

Weisman, M. L., and J. B. Klemp, 1986: Characteristics of isolated convective storms. *Mesoscale Meteorology and Forecasting*, P. S. Ray, Ed., Amer. Meteor. Soc., Boston, 331–358.